Phase separation of Myc differentially regulates gene transcription

Junjiao Yang[1, 2, 3], Chan-I Chung[1, 2, 3], Jessica Koach[4], Hongjiang Liu[5], Qian Zhao[1, 2], Xiaoyu Yang[5], Yin Shen[5], William A. Weiss[4], Xiaokun Shu[1, 2, *]

[1]Department of Pharmaceutical Chemistry, University of California, San Francisco, San Francisco, California, USA.

[2]Cardiovascular Research Institute, University of California, San Francisco, San Francisco, California, USA

[3]These authors contributed equally.

[4]Departments of Neurology, Neurological Surgery, Pediatrics, and Helen Diller Family Comprehensive Cancer Center, University of California, San Francisco, San Francisco, CA, USA.

[5]Institute for Human Genetics, Departments of Neurology, Weill Institute for Neurosciences, University of California, San Francisco, San Francisco, CA, USA.

[*]Correspondence to: Xiaokun Shu (email: xiaokun.shu@ucsf.edu)

Abstract

Dysregulation and enhanced expression of *MYC* transcription factors including *MYC* and *MYCN* contribute to majority of human cancers. For example, *MYCN* is amplified up to several hundred-fold in high-risk neuroblastoma. One potential consequence of elevated expression is liquid-liquid phase separation (LLPS), occurring when the concentration of certain macromolecules and biopolymers is above a threshold. Here, we show that in *MYCN*-amplified human neuroblastoma cells, N-myc protein forms condensate-like structures. Using *MYCN*-nonamplified neuroblastoma cells that have no or little endogenous N-myc protein expression, we found that exogenously expressed N-myc undergoes LLPS in a concentration-dependent manner, and determined its threshold concentration for LLPS in the cellular context. Biophysically, N-myc condensates in live cells exhibit liquid-like behavior. The intrinsically disordered transactivation domain (TAD) of N-myc is indispensable for LLPS. Functionally, the N-myc condensates contain its obligatory DNA-binding and dimerization partner, genomic DNA, transcriptional machinery, and nascent RNA. These condensates are dynamically regulated during cell mitosis, correlated with chromosomal condensation and de-condensation. We further show that the TAD and the DNA-binding domain are both required for transcriptional activity of N-myc condensates. Most importantly, using a chemogenetic tool that decouples the role of phase separation from changes in protein abundance level in the nucleus, we discovered that N-myc phase separation regulates gene transcription and promotes SH-EP cell proliferation. Interestingly, LLPS of N-myc only modulates a small proportion of N-myc-regulated genes. Taken together, our results demonstrate that N-myc undergoes LLPS, and that its phase separation differentially modulates the transcriptome, partially contributes to gene transcription, and promotes cell proliferation. Our work opens a new direction in understanding Myc-related cancer biology that has been studied for several decades.

MYC family transcription factors are major contributors to human tumorigenesis. Expression of Myc is deregulated and enhanced in many types of cancers, due to copy number changes, chromosomal translocations, and upstream oncogenic signaling [1-3]. For instance, *MYCN* is highly amplified up to 100-to-300 fold in nearly half of high-risk neuroblastoma [4-7]. While upregulated Myc expression induces tumor development in many tissues, depletion of Myc abolishes tumorigenesis and results in tumor regression in various tumor models [8-12]. One potential consequence of elevated protein expression is phase separation, which is dependent on protein concentration[13-17]. Recently, many transcription factors that contain intrinsically disordered regions (IDR) have been reported to undergo LLPS, forming biomolecular condensates (also known as membraneless compartments, granules, or liquid droplets) when protein concentration surpass a threshold concentration [18-21]. Biomolecular condensates compartmentalize interacting proteins and signaling complexes [14-16,21-24]. Condensates of many transcriptional factors have been proposed and demonstrated to compartmentalize transcriptional machinery and to remodel gene transcription [18-21,25].

Myc oncoproteins are transcription factors with N-terminal TAD domains containing an IDR. Purified recombinant c-Myc-mEGFP has been shown to form condensates at high concentration (12 μM), and partitions into MED1-IDR condensates [19]. On the other hand, it remains unknown whether Myc undergoes phase separation in living cells, whether the condensates have liquid properties and if they are transcriptionally active in living cells. Because neuroblastoma cells often contain highly amplified *MYCN*, we conducted immunostaining of N-myc in the *MYCN*-amplified Kelly neuroblastoma cells, observing punctate structures in the nuclei of these cancer cells. Next, we conducted live cell imaging using mEGFP tagged N-myc in the *MYCN*-nonamplified SH-EP neuroblastoma cells that have no or little endogenous N-myc protein expression. The imaging data showed that N-myc undergoes LLPS in a concentration-dependent manner. The N-myc condensates possess liquid-like behavior, compartmentalize transcriptional machinery and contain nascent RNAs.

In addition to the important question of whether Myc condensates are transcriptionally active, another critical question to answer is whether phase separation plays a role in transcription, which has been challenging to investigate for the field of biomolecular condensate. This is because, on the one hand, protein phase separation is a concentration-dependent phenomena. A bio-condensate forms when protein abundance level exceeds a threshold. On the other hand, the protein abundance of transcription factors in the nucleus affects transcriptional activity. For example, protein level increase of YAP in the nucleus via cytoplasm-nuclear shuttling activates its transcription. It is thus critical to decouple role of phase separation from changes in protein abundance in the nucleus. Ideally, the role of phase separation should be determined by comparing activities of transcription factors in the homogenously distributed state (i.e. dilute phase) versus condensed phase, with protein level of transcription factors in the nucleus maintained constant. Measurement of transcriptional activity when transcriptional factors undergo such spatial reorganization will define role of phase separation on transcription.

Here we applied a chemogenetic tool to drive N-myc phase separation from the dilute phase to condensed phase without changing the N-myc protein level in the nucleus, which decouples the role of phase separation from changes in protein abundance. This enables us to determine role of N-myc phase separation on transcription. Our work reveals that while N-myc phase separation

indeed regulates transcription, only 6% of target genes are regulated by phase separation. These results suggest that phase separation differentially modulates the transcriptome, opening a new direction in understanding Myc-related cancer biology.

RESULTS

N-myc undergoes liquid-liquid phase separation in cells

We first imaged N-myc in *MYCN*-amplified human Kelly neuroblastoma cells. Immunofluorescence imaging indicated that N-myc protein formed puncta in the nucleus (Fig. 1a), which were not observed upon treatment with the MYC/MAX dimerization inhibitor [26] (Supporting Fig. S1). Importantly, in *MYCN*-nonamplified SH-EP and CLB-GA neuroblastoma cells, we did not observe obvious punctate structures based on immunofluorescence (Supporting Fig. S2), suggesting that formation of N-myc puncta is dependent on its expression levels because CLB-GA and SH-EP has no or little expression of endogenous N-myc (Supporting Fig. S3). To further characterize N-myc, we conducted live-cell imaging of the SH-EP cells. We fused mEGFP to N-myc (N-myc-mEGFP), which was exogenously expressed in SH-EP cells. Fluorescence imaging of single cells showed that N-myc-mEGFP formed puncta in a concentration-dependent manner. In particular, N-myc-mEGFP was evenly distributed and did not form punctate structures until its expression level was above a threshold concentration (i.e. saturation concentration) (Fig. 1b).

To quantitively analyze the data, we determined the percentage of N-myc in punctate structures over total in single cells by defining SPARK signal, which is the ratio of summarized fluorescence intensity of N-myc in the puncta (i.e. amount of N-myc in the punctate structure) divided by summarized fluorescence intensity of total N-myc in each cell. Our data showed that N-myc formed punctate structures with threshold or saturation concentration ~ 300 – 400 nM (here the protein concentration was estimated based on purified mEGFP, see Methods and Supporting Fig. S4). Briefly, below the saturation concentration, e.g. at ~ 250 nM, N-myc was evenly distributed in the nucleus (Fig. 1b, upper-right). Above the saturation concentration, e.g. at ~500 nM, N-myc formed puncta in the nucleus (Fig. 1b, lower-right). Thus, our data shows that N-myc-mEGFP undergoes concentration-dependent spatial reorganization. We estimated that the N-myc concentration is around 0.7 – 1 μM in the Kelly cells (Supporting Fig. S5). We also characterized relationship of number and size of the N-myc puncta to the protein levels. The number of N-myc puncta increases as N-myc protein level increases (Supporting Fig. S6A). The size of N-myc puncta is in the range of 0.4 – 1 μm (diameter), and this distribution is independent of the protein levels (Supporting Fig. S6B). This suggests that N-myc tends to form new puncta when the protein level increases.

Next, we determined whether the N-myc puncta exhibit liquid-like properties. We conducted time-lapse imaging and characterized fusion events between the punctate structures. These puncta can fuse and coalesce within a few seconds. The fusing puncta initially formed a dumbbell shape, which over time relaxed to a spherical shape (Fig. 1c). Quantitative analysis showed that aspect ratio of the fusing puncta over time fits well to a single exponential curve (Fig. 1c, lower left), which is a well-known characteristic of coalescing liquid droplets [27,28]. Furthermore, we used this data to determine inverse capillary velocity ($= \eta/\gamma$; here γ is surface tension of the droplet; η is viscosity), which was 1.2 ± 0.2 (s/μm) (Fig. 1c, lower right). Thus, quantitative analysis of the fusion events indicated that the punctate structures of N-myc contain

liquid properties and thus they are liquid droplets. This suggests that N-myc-mEGFP undergoes LLPS, forming liquid-like condensates when its concentration exceeds above the threshold.

The Myc TAD domain, which spans the N-terminal conserved motifs, including three "Myc boxes" (MB0-II) from 1 to 137 residues (for N-myc, which totals 464 residues), is intrinsically disordered [29,30]. To examine role of the TAD in N-myc LLPS, we designed and characterized a TAD truncation mutant (N-myc$^{138\text{-}464}$). Live cell imaging revealed that this mEGFP-tagged fusion protein (N-myc$^{138\text{-}464}$-mEGFP) no longer formed condensates even above 2 μM concentration (Fig. 1d), ~ 5-fold above the threshold concentration of LLPS for full length N-myc. Therefore, our data demonstrate that N-myc LLPS depends on the IDR-containing TAD, consistent with LLPS of many other proteins that also rely on their IDR.

N-myc condensates contain DNA-binding partner MAX and genomic DNA

To examine whether the N-myc condensates are transcriptionally active, we first determined that N-myc condensates contain the obligatory DNA-binding partner MAX. To visualize MAX in living cells, we labeled it with a red fluorescent protein mKO3. Multicolor fluorescence imaging showed that MAX also formed condensates in cells that contained N-myc condensates, and that the green N-myc condensates colocalized with the red MAX condensates (Fig. 2A). In cells without N-myc-mEGFP, MAX did not form condensates (Supporting Fig. S7). These data suggest that N-myc condensates recruit its DNA-binding partner MAX.

Next, we determined that the N-myc condensates contained genomic DNA of the N-myc target gene *p53* [31,32]. We labeled the *p53* DNA using fluorescence in situ hybridization (FISH). Confocal fluorescence imaging revealed that N-myc condensates were associated with the genomic DNA of *p53* (Fig. 2B). These data suggest that the N-myc condensates bind genomic DNA, consistent with the above results that these condensates contain the DNA-binding partner MAX. Thus, the N-myc condensates have a potential to activate gene transcription.

N-myc condensates contain transcriptional machinery and nascent RNA

Next, we determined that N-myc condensates contain transcriptional machinery, including the Mediator and RNA polymerase II (Pol II). First, immunofluorescence imaging showed that the Mediator of RNA polymerase II transcription subunit 1 (MED1) formed condensates, consistent with previous studies. Furthermore, N-myc condensates colocalized with MED1 condensates (Fig. 2C), indicating that N-myc condensates contain MED1. Second, we stained the cells with antibodies against phosphorylated Pol II at Ser5 (Pol II S5p) at the C-terminal domain. Immunofluorescence imaging showed punctate structures of Pol II S5p, which colocalized with N-myc condensates based on two-color imaging (Fig. 2D). Therefore, our data indicate that N-myc condensates contain Pol II. We also imaged Kelly cells and showed that N-myc puncta colocalized with MED1 and Pol II (Supporting Fig. S8).

We next determined that the N-myc condensates contained nascent RNA. We incubated cells with uridine analog 5-ethynyluridine (EU) for 1 hour so that EU was incorporated into newly transcribed RNA. The EU-labeled nascent RNA was detected through a copper (I)-catalyzed cycloaddition reaction (i.e. "click" chemistry) using azides labeled with red fluorescent dyes [33]. Fluorescence imaging revealed several punctate structures (Fig. 2E). The round structures of

nascent RNAs colocalized with the N-myc condensates, suggesting that these N-myc condensates contain nascent RNAs.

Lastly, we quantified the colocalization of N-myc condensates with MAX, MED1, Pol II S5p and nascent RNAs (Fig. 2F, Methods). We calculate that ~92% of N-myc condensates contained MAX. The percentage of N-myc condensates that contain MED1, Pol II S5p and nascent RNAs is ~ 72%, 62%, 80%, respectively.

N-myc condensates are dynamically regulated during cell mitosis.

Because many biomolecular condensates disassemble during mitosis [34], we examined whether N-myc condensates were also regulated dynamically during cell cycle. Live-cell fluorescence imaging showed that N-myc condensates dissolved when cells entered mitosis (Fig. 3A, left panel). Upon mitotic entry, chromatin condenses even though nuclear chromatin is already compacted in the interphase. It has been well established that many transcription factors disengage from chromatin when cells enter mitosis. We thus decided to investigate the relationship between N-myc condensate dissolution and chromatin condensation upon entry into mitosis. To visualize chromatin, we labeled histone 2B (H2B) with a near-infrared fluorescent protein mIFP. This allowed us to quantify volume of chromatin using fluorescent protein labeled H2B [35]. Time-lapse imaging revealed that dissolution of N-myc condensates preceded chromatin condensation by ~ 6 minutes (Fig. 3A, right panel). The dissolution of N-myc condensates also occurred before nuclear breakdown (Fig. 3A, T ~ 16 min.).

Next, we examined whether N-myc reformed condensates when cells exit mitosis. Time-lapse imaging revealed that indeed upon mitotic exit, N-myc condensates reappeared. We also observed that chromatin decondensed during mitotic exit, consistent with previous studies [35]. Interestingly, during mitotic exit, N-myc condensate formed after chromatin decondensation with a delay of ~ 6-minutes (Fig. 3B). This contrasts mitotic entry, where dissolution of N-myc condensates occured before chromatin condensation. These results are biologically consistent however, as when the chromatin condenses during mitosis, N-myc condensates dissolve; but when chromatin decondenses during interphase, N-myc condensates reassemble.

Our study thus reveals that N-myc condenates are dynamically regulated during mitosis, and that the condensate disassembly and reassembly is correlated with chromatin condensation and de-condensation, respectively. Because many transcription factors disengage from chromatin when cells enter mitosis and re-associate with chromatin when cells exit mitosis, we investigated a potential role of the N-myc DNA binding domain bHLH-LZ (366-464 aa) on N-myc phase separation. We truncated bHLH-LZ and measured phase separation of this truncation mutant N-myc$^{1\text{-}365}$. Indeed, the saturation concentration of this mutant is ~ 620 – 720 nM (Fig. 3C, blue box), which is ~ 2-fold more than the saturation concentration of N-myc (~ 300 – 400 nM, Fig. 1B; red box in Fig. 3C). Our data thus suggest that the DNA binding domain plays a critical role and contributes to N-myc phase separation, which likely explains the dynamic regulation of N-myc condensates during mitosis.

Transcriptional activity of N-myc condensates requires both TAD and bHLH-LZ domains

Because our data indicate that both the TAD and bHLH-LZ domains are important for N-myc LLPS, we examined whether both domains were required for transcriptional activity of N-myc

condensates. Here we applied a chemogenetic tool named SparkDrop to drive phase separation of both N-myc mutants (Fig. 4A). SparkDrop drives protein phase separation by a small molecule-induced multivalent interaction. Briefly, SparkDrop is based on a newly engineered protein pair CEL (109 amino acids [aa]) and ZIF (31aa), which, upon addition of lenalidomide (lena), form a heterodimer (CEL⋯lena⋯ZIF). To induce LLPS, we fused the N-myc mutants to mEGFP and CEL (N-myc-mEGFP-CEL). To incorporate multivalency, we utilized a de novo designed coiled coil that is a homo-tetramer (HOTag6). We fused ZIF, a nuclear localization signal (NLS), and a non-green fluorescent EGFP mutant (EGFP-Y66F) to HOTag6 (ZIF-NLS-EGFP(Y66F)-HOTag6).

First, we demonstrated that SparkDrop induced phase separation of TAD-deleted N-myc$^{138\text{-}464}$ upon addition of lenalidomide (Fig. 4A). The condensates recruited the DNA-binding partner MAX as expected (Fig. 4B). In contrast, most of the N-myc condensates did not contain MED1 (Fig. 4C) or Pol II S5p (Supporting Fig. S9A). Most (98%) of the N-myc condensates contained MAX, whereas Med1 and Pol II S5 P showed ~5% and 0.4% colocalization, respectively (Fig. 4D). These data thus suggest that the TAD domain is critical for transcriptional activity of N-myc condensates.

Next, we showed that SparkDrop was also able to drive phase separation of bHLH-LZ-deleted N-myc$^{1\text{-}365}$ (Fig. 4E). The majority of these condensates contained no MED1 or Pol II S5p, ~13% and ~4% colocalization, respectively (Fig. 4F, Supporting Fig. S9B), indicating that they are largely inactive in gene transcription. As expected, these condensates contained no MAX (Fig. 4F). Therefore, our data suggest that the DNA-binding domain is also critical for transcriptional activity of N-myc condensates. Together, our results indicate that the transcriptional activity of N-myc condensates requires both the TAD and the DNA-binding domains, and that without the TAD or the DNA-binding domain of N-myc, condensate formation itself does not recruit the transcriptional machinery.

The chemogenetic tool SparkDrop decouples N-myc LLPS from protein abundance

While we have demonstrated that N-myc undergoes LLPS and forms liquid condensates, and that these condensates are transcriptionally active, another key question is whether phase separation, i.e. condensate formation itself, promotes or regulates gene transcription. Protein condensate formation can be divided into two steps: 1) protein level increase above saturation concentration; 2) phase separation, which is essentially a spatial reorganization from a homogenous distribution (dilute phase) to a condensed state or phase. The abundance of a transcription factor (e.g. YAP) is known to regulate transcription. Therefore, to understand role of phase separation, it is essential to decouple phase separation from protein abundance.

Here, we turned to the chemogenetic tool SparkDrop that enables us to drive LLPS without changing protein levels, thus decoupling phase separation from protein abundance. We tagged N-myc by SparkDrop (N-myc/SparkDrop) and demonstrated that SparkDrop induced phase separation of N-myc without change of protein levels, and that the induced N-myc/SparkDrop condensates are liquid droplets. In particular, we first showed that lenalidomide-activatable SparkDrop induced N-myc condensate formation within 6 – 10 minutes (Fig. 5A). The total fluorescence of N-myc showed little change during phase separation, suggesting that N-myc protein level was constant in the nucleus. Two negative controls showed that DMSO did not

induce N-myc phase separation, and that lenalidomide alone could not drive N-myc phase separation using the N-myc/SparkDrop control (no HOTag6). Furthermore, without N-myc, SparkDrop did not form droplets upon addition of lenalidomide (Fig. S11). We also demonstrated that in the absence of lenalidomide, N-myc/SparkDrop undergoes LLPS with saturation concentration ~330 – 400 nM (Supporting Fig. S10), similar to that of N-myc-mEGFP, indicating that the SparkDrop tag itself had little effect on N-myc's phase separation properties. Lastly, we showed that the N-myc/SparkDrop condensates were able to fuse and coalesce together, indicating that they are liquid droplets (Supporting Fig. S12).

Next, we determined that N-myc/SparkDrop condensates are transcriptionally active. First, the N-myc/SparkDrop condensates contained the DNA-binding and dimerization partner MAX, with colocalization ~ 95% (Fig. 5B). Second, the N-myc/SparkDrop condensates contained transcriptional machinery including MED1 and Pol II S5p (Fig. 5C, D). Lastly, the N-myc/SparkDrop condensates contained nascent RNA (Fig. 5F). Colocalization of MAX, MED1, Pol II S5, and nascent RNA to N-myc condensates was 95%, 85%, 72%, and 80%, respectively (Fig. 5F). These data thus suggest that SparkDrop decouples phase separation from protein levels, and that the SparkDrop-induced N-myc condensates are transcriptionally active in cells, paving the way for investigating functional roles of phase separation.

LLPS of N-myc regulates cell proliferation and gene transcription

We first determined that phase separation of N-myc promotes cell proliferation. Here we engineered SH-EP cells that stably express N-myc/SparkDrop. We measured cell proliferation rate and found that it increased by 15 $\pm$ 4% when N-myc formed condensates using lenalidomide-activatable SparkDrop in comparison to the DMSO-treated cells that contained N-myc in the dilute phase (Fig. 5G, H). Furthermore, we also conducted control experiments with the N-myc/SparkDrop control (no HOTag6), which showed that lenalidomide alone had little effect on cell proliferation.

Next, we examined whether phase separation of N-myc regulated gene transcription. Here, we treated the stable cells with or without lenalidomide, which showed condensed or dilute phase of N-myc, respectively (Fig. 5H). Western blot analysis confirmed that the protein levels of N-myc showed little difference between the dilute and the condensed phase (Fig. 5I). Furthermore, mRNA level of *MYCN* also showed little change upon N-myc phase separation, based on the RNA-sequencing (RNA-seq) analysis (see next section). We chose two N-myc-regulated genes serine incorporator 2 (SERINC2) and annexin A8 (ANXA8) to examine if their transcription is regulated upon N-myc phase separation. RT-qPCR analysis revealed that the mRNA levels of SERINC2 and ANXA8 were significantly higher for the condensed N-myc than the dilute N-myc (Fig. 5J). These results suggest that N-myc phase separation increases transcription of these genes. As a control, we showed that lenalidomide alone did not affect transcription of these two genes (Fig. 5J), based on the N-myc/SparkDrop control (no HOTag6), which did not form condensates upon addition of lenalidomide (Fig. 5H). Therefore, our data indicate that N-myc phase separation regulates transcriptional activity and promotes proliferation of SH-EP cells.

N-myc phase separation differentially modulates the transcriptome

To further understand how phase separation of N-myc affects global gene transcription, we conducted RNA-seq analysis. By comparing the RNA-seq data of N-myc in condensed phase

versus those of N-myc in dilute phase, we calculated statistically significant DE (differentially expressed) genes (DEGs; p-value < 0.01, FDR < 0.1), which revealed global changes of gene expression upon N-myc phase separation (while N-myc expression was at the same level) (Fig. 6A, B). These genes have modest change in magnitude, consistent with typical changes of Myc-regulated genes [36]. As a control, we confirmed that lenalidomide itself had little effect on N-myc transcription because only 4 DEGs overlapped with DEGs by N-myc LLPS (Fig. 6C, Supporting Fig. S14). LLPS-regulated DEGs include 660 genes (Supporting Fig. S13, supporting excel file 1). Gene ontology (GO) enrichment analysis reveals that the LLPS-regulated genes are strongly linked to several Myc-related biological processes including cell adhesion, ribosomal biogenesis, and cell differentiation (Fig. 6D).

While N-myc phase separation regulated 660 genes, our data showed that phase separation had no large impact on the global transcriptomic signature of N-myc. We compared the DEGs of N-myc in the condensed phase versus those of N-myc in the dilute phase (Fig. 6E, supporting excel files 2 and 3), which showed that the transcriptomic signature is largely unchanged. Furthermore, we compared phase separation-regulated genes with N-myc (dilute phase)-regulated genes (Fig. 6F), which revealed that phase separation modulates fewer than 6% of N-myc-regulated genes. Therefore, our data indicate that phase separation selectively or differentially regulates N-myc transcription, while maintaining the global transcriptomic signature of N-myc. As a control, we verified that lenalidomide itself had little effect on N-myc transcription because only 10 out of 9411 genes regulated by N-myc overlap with those regulated by lenalidomide itself (Supporting Fig. S15). In total, there are 11 DEGs regulated by lenalidomide alone by calculating DEGs from N-myc/SparkDrop control (no HOTag6) with lenalidomide versus DMSO (Supporting excel file 4).

Because Myc (including N-myc) and MAX heterodimer binds E-box and many Myc regulated genes are reported to contain E-box motif [37], we conducted E-box enrichment analysis between the LLPS-regulated and LLPS-independent genes. First, when we include all of the LLPS-regulated genes regardless of fold change, E-box is slightly enriched but it is not statistically significant with p-value = 0.06 (Fig. 6G). Next, we divided the LLPS-regulated genes into two groups according to fold change: a strongly regulated group and a weakly regulated group. The strongly regulated group contain LLPS-regulated genes with $|Log_2FC| > 0.3$, while the weakly regulated group contain LLPS-regulated genes with $|Log_2FC| < 0.3$. The strongly regulated group shows significant E-box enrichment (p-value < 0.001). In contrast, the weakly-regulated group does not show E-box enrichment (p-value = 0.69). Furthermore, when we compared the strongly regulated group against the weakly regulated group, E-box is also significantly enriched (p-value < 0.01). These data suggest that regulation of gene transcription by N-myc LLPS is correlated with E-box enrichment. The genes with relatively strong regulation by LLPS are enriched with the E-box motif over the LLPS-independent or weakly regulated genes.

Lastly, we examined a previous list of 41 core genes of Myc [38], and found that 38 out of 41 were regulated in the SH-EP cells with dilute phase N-myc/SparkDrop (Supporting Fig. S16). This suggests that the SparkDrop system had little perturbation on the core transcriptional function of N-myc. Therefore, our SparkDrop-based approach is appropriate for identifying the genes that are regulated by N-myc LLPS. SparkDrop is thus a versatile chemogenetic tool for studying the role of phase separation for many other transcriptional factors.

Discussion

MYC undergoes LLPS forming liquid droplets. Recently, several studies have revealed important roles of oncoprotein condensates in oncogenic signaling and transcription [39-46]. In this work, we examined the MYC transcription factor N-myc and found that N-myc formed punctate structures in *MYCN*-amplified human neuroblastoma cells, suggesting that N-myc may form condensates when it is highly expressed. To further examine N-myc condensates in living cells, we tagged N-myc by mEGFP and exogenously expressed the fusion protein N-myc-mEGFP in the *MYCN*-nonamplified neuroblastoma SH-EP cells that have no or little endogenous N-myc expression. Our single cell analysis showed that N-myc undergoes concentration-dependent LLPS, and we determined the threshold concentration for LLPS at ~ 300 – 400 nM. Using time-lapse imaging, we further established that N-myc condensates contain liquid-like properties. The inverse capillary velocity of these fusing droplets was ~ 55% of that of P granules [47], and ~30 to 80 times lower than that of nucleoli [27,28].

N-myc condensates are transcriptionally active. One of the key questions in the condensate biology field is whether the biomolecular condensates are biologically active. Here we determined that the N-myc condensates are transcriptionally active, because they compartmentalize the DNA-binding and dimerization partner MAX, genomic DNA of its target gene p53, transcriptional machinery including the Mediator complex and RNA Pol II. These condensates also contain nascent RNAs. Most importantly, using the chemogenetic tool SparkDrop, we determined that N-myc condensates regulate transcription.

Here, SparkDrop drives protein phase separation without changing the abundance of N-myc protein in the nucleus. Thus, SparkDrop decouples the role of phase separation on transcription, from increased protein levels that are well known to affect transcription. Our data not only reveal that N-myc condensates are transcriptionally active, but also that phase separation of N-myc contributes to transcription. Phase separation is essentially a spatial reorganization from homogenously distributed dilute phase to condensed phase. Our results suggest that such spatial reorganization of N-myc in the nucleus can affect gene transcription. Thus, our work shows that it is biologically important to examine role of phase separation for transcription factors.

N-myc phase separation and transcriptional activity requires TAD and chromatin binding. Many studies report that protein phase separation often requires the intrinsically disordered region. Here we also showed that N-myc LLPS requires the intrinsically disordered TAD. Furthermore, we also discovered that the DNA-binding domain of N-myc also contributes to phase separation, because lack of the bHLH-LZ domain increased the threshold concentration for LLPS. Consistently, we found that N-myc LLPS was dynamically regulated during cell mitosis when most transcription factors disengage from chromatin. The N-myc condensates disassembled when cells entered mitosis and reassembled upon mitotic exit. Furthermore, this dynamic regulation is correlated with chromosomal changes during mitosis. The N-myc condensates dissolve ~ 6 minutes before chromosome condensation upon mitotic entry. Upon mitotic exit, the N-myc condensates reformed ~ 6 minutes after chromosome de-condensation.

Other biomolecular condensates known to dissolve during mitosis include cytosolic condensates such as stress granules and P-bodies, as well as nuclear condensates such as nucleoli and nuclear speckles[34]. While recent work has unveiled regulatory mechanisms of condensates such as stress granules, for many other condensates, it remains unclear how their LLPS is regulated during mitosis [34]. Here, we discovered that disassembly and reassembly of the N-myc condensates correlated with chromosome condensation and de-condensation, respectively. While chromosomes are already compacted in interphase, they are further condensed during mitosis. It is well established that transcription mostly stops during mitosis. Most transcription factors dissociate from the condensed chromosomes when cells enter mitosis, and reassociate with decondensed chromosomes upon mitotic exit [48-50].

Phase separation of N-myc differentially regulates transcriptome. Biomolecular condensates form via phase separation when protein levels exceed a threshold concentration. Arguably, the most important and challenging question that remains mostly unanswered in the condensate biology field is whether phase separation confers new or additional biological functions or activities, such as affecting gene transcription by transcription factors. Furthermore, does phase separation of a transcription factor equally or differentially regulate its downstream genes? Protein condensate formation is composed of two steps:1) protein level increase; 2) phase separation, which is essentially a spatial reorganization from a homogenous distribution (dilute phase) to a condensate state (condensed phase). Protein level increase of a transcription factor (e.g. YAP) is known to regulate transcription. Therefore, to understand role of phase separation, it is essential to decouple phase separation from increased protein levels.

Here, we utilized the chemogenetic tool SparkDrop that drives protein phase separation without changing protein levels, to manipulate N-myc phase separation in living cells. SparkDrop enables decoupling of N-myc phase separation from its abundance in the nucleus. Using the neuroblastoma SH-EP cell as a model, we show that phase separation of N-myc does contribute to transcription, and even more interestingly, it modulates a small percentage of genes (< 6%) out of the several thousand regulated by N-myc. The LLPS-regulated genes with relatively large fold change are significantly enriched with the E-box motif over the LLPS-independent or weakly regulated genes. This suggests that N-myc LLPS may exert transcriptional regulation by interacting with E-box motifs. Taken together, our work indicates that N-myc phase separation does regulate gene transcription (likely through the E-box), and more interestingly, it differentially regulates transcriptome with little change of the global transcriptomic signature.

In summary, our work establishes that N-myc undergoes LLPS in live cells, forming liquid-like condensates that are transcriptionally active. Phase separation of N-myc differentially modulates transcriptome, and partially contributes to transcription of many genes. Consistently, N-myc LLPS promotes cell proliferation. While these encouraging results may only be able to answer a small portion of Myc-related questions, our work opens new directions to spur future studies in understanding important Myc-related cancer biology that has been studied for several decades.

Acknowledgments: We thank Hiten Madhani, Vijay Ramani, and Eric Holland for critical suggestions.
Funding: This work was supported by NIH R01CA258237 and U01DK127421 (to X.S.), and NIH P01CA217959, P30CA082103, U01CA217864, and grants from the Alex Lemonade Stand, St. Baldrick, and Samuel Waxman Cancer Research Foundations (to W.A.W.), and U01DA052713 (to Y.S.).
Author contributions: X.S. conceived the project. X.S., J.Y., C-I.C designed the experiments and composed the manuscript. J.Y. performed N-myc phase separation and colocalization with other proteins in cells. C-I.C. conducted imaging of small molecule induced N-myc phase separation and analyzed colocalization with other proteins. C-I.C. performed and analyzed nascent RNA labeling, RT-qPCR and RNA-seq. J.K. and W.A.W planned and performed experiments to analyze expression of endogenous N-myc protein in the neuroblastoma cells. H.L. processed RNA-seq data. H.L., C-I.C, J.Y., Q.Z., X.Y., X.S., Y.S. analyzed RNA-seq data. All authors contributed to the final draft.
Competing interests: X.S. and W.A.W. are co-founders of Granule Therapeutics.
Data and materials availability: All data are available in the main text or the supplementary materials.
Code Availability: All relevant codes are available upon request.

Supplementary Materials:

Materials and Methods

Figures S1-S16

Supporting excel files 1 – 4 (list of DEGs from RNA-seq)

References

1. Baluapuri, A., Wolf, E. & Eilers, M. Target gene-independent functions of MYC oncoproteins. *Nat Rev Mol Cell Biol* 1–13 (2020). doi:10.1038/s41580-020-0215-2
2. Dang, C. V. MYC on the Path to Cancer. *Cell* **149,** 22–35 (2012).
3. Meyer, N. & Penn, L. Z. Reflecting on 25 years with MYC. *Nat Rev Cancer* **8,** 976–990 (2008).
4. Cheng, J. M. *et al.* Preferential amplification of the paternal allele of the N-myc gene in human neuroblastomas. *Nat Genet* **4,** 191–194 (1993).
5. Brodeur, G. M., Seeger, R. C., Schwab, M., Varmus, H. E. & Bishop, J. M. Amplification of N-myc in Untreated Human Neuroblastomas Correlates with Advanced Disease Stage. *Science* **224,** 1121–1124 (1984).
6. Kohl, N. E., Gee, C. E. & Alt, F. W. Activated expression of the N-myc gene in human neuroblastomas and related tumors. *Science* **226,** 1335–1337 (1984).
7. Pugh, T. J. *et al.* The genetic landscape of high-risk neuroblastoma. *Nat Genet* 1–9 (2013). doi:10.1038/ng.2529
8. Chanthery, Y. H. *et al.* Paracrine signaling through MYCN enhances tumor-vascular interactions in neuroblastoma. *Science Translational Medicine* **4,** 115ra3–115ra3 (2012).
9. Murphy, D. J. *et al.* Distinct Thresholds Govern Myc's Biological Output In Vivo. *Cancer Cell* **14,** 447–457 (2008).
10. Soucek, L. *et al.* Modelling Myc inhibition as a cancer therapy. *Nature* **455,** 679–683 (2008).
11. Smith, D. P., Bath, M. L., Metcalf, D., Harris, A. W. & Cory, S. MYC levels govern hematopoietic tumor type and latency in transgenic mice. *Blood* **108,** 653–661 (2006).
12. Felsher, D. W. & Bishop, J. M. Reversible tumorigenesis by MYC in hematopoietic lineages. *Mol Cell* **4,** 199–207 (1999).
13. Choi, J.-M., Holehouse, A. S. & Pappu, R. V. Physical Principles Underlying the Complex Biology of Intracellular Phase Transitions. *Annual review of biophysics* **49,** annurev–biophys–121219–081629–27 (2020).
14. Wheeler, R. J. & Hyman, A. A. Controlling compartmentalization by non-membrane-bound organelles. *Philosophical Transactions of the Royal Society B: Biological Sciences* **373,** 20170193–9 (2018).
15. Banani, S. F., Lee, H. O., Hyman, A. A. & Rosen, M. K. Biomolecular condensates: organizers of cellular biochemistry. *Nat Rev Mol Cell Biol* 1–14 (2017). doi:10.1038/nrm.2017.7
16. Hyman, A. A., Weber, C. A. & Jülicher, F. Liquid-Liquid Phase Separation in Biology. *Annu Rev Cell Dev Biol* **30,** 39–58 (2014).
17. Hyman, A. A. & Simons, K. Cell biology. Beyond oil and water--phase transitions in cells. *Science* **337,** 1047–1049 (2012).
18. Zamudio, A. V. *et al.* Mediator Condensates Localize Signaling Factors to Key Cell Identity Genes. *Mol Cell* 1–2 (2019). doi:10.1016/j.molcel.2019.08.016
19. Boija, A. *et al.* Transcription Factors Activate Genes through the Phase-Separation Capacity of Their Activation Domains. *Cell* **175,** 1842–1855.e16 (2018).
20. Chong, S. *et al.* Imaging dynamic and selective low-complexity domain interactions that control gene transcription. *Science* **361,** eaar2555–11 (2018).

21. Hnisz, D., Shrinivas, K., Young, R. A., Chakraborty, A. K. & Sharp, P. A. Perspective. *Cell* **169,** 13–23 (2017).
22. Lyon, A. S., Peeples, W. B. & Rosen, M. K. A framework for understanding the functions of biomolecular condensates across scales. *Nat Rev Mol Cell Biol* 1–21 (2021). doi:10.1038/s41580-020-00303-z
23. Alberti, S. & Hyman, A. A. Biomolecular condensates at the nexus of cellular stress, protein aggregation disease and ageing. *Nat Rev Mol Cell Biol* 1–18 (2021). doi:10.1038/s41580-020-00326-6
24. Shin, Y. & Brangwynne, C. P. Liquid phase condensation in cell physiology and disease. *Science* **357,** eaaf4382 (2017).
25. Li, C. H. *et al.* MeCP2 links heterochromatin condensates and neurodevelopmental disease. *Nature* 1–28 (2020). doi:10.1038/s41586-020-2574-4
26. Han, H. *et al.* Small-Molecule MYC Inhibitors Suppress Tumor Growth and Enhance Immunotherapy. *Cancer Cell* 1–31 (2019). doi:10.1016/j.ccell.2019.10.001
27. Feric, M. *et al.* Coexisting Liquid Phases Underlie Nucleolar Subcompartments. *Cell* **165,** 1686–1697 (2016).
28. Brangwynne, C. P., Mitchison, T. J. & Hyman, A. A. Active liquid-like behavior of nucleoli determines their size and shape in Xenopus laevis oocytes. *Proceedings of the National Academy of Sciences* **108,** 4334–4339 (2011).
29. Andresen, C. *et al.* Transient structure and dynamics in the disordered c-Myc transactivation domain affect Bin1 binding. *Nucleic Acids Res* **40,** 6353–6366 (2012).
30. McEwan, I. J., Dahlman-Wright, K., Ford, J. & Wright, A. P. Functional interaction of the c-Myc transactivation domain with the TATA binding protein: evidence for an induced fit model of transactivation domain folding. *Biochemistry* **35,** 9584–9593 (1996).
31. Chen, L. *et al.* p53 is a direct transcriptional target of MYCN in neuroblastoma. *Cancer Res* **70,** 1377–1388 (2010).
32. Reisman, D., Elkind, N. B., Roy, B., Beamon, J. & Rotter, V. c-Myc trans-activates the p53 promoter through a required downstream CACGTG motif. *Cell Growth Differ* **4,** 57–65 (1993).
33. Jao, C. Y. & Salic, A. Exploring RNA transcription and turnover in vivo by using click chemistry. *Proceedings of the National Academy of Sciences* **105,** 15779–15784 (2008).
34. Rai, A. K., Chen, J.-X., Selbach, M. & Pelkmans, L. Kinase-controlled phase transition of membraneless organelles in mitosis. *Nature* 1–25 (2018). doi:10.1038/s41586-018-0279-8
35. Vagnarelli, P. Mitotic chromosome condensation in vertebrates. *Exp Cell Res* **318,** 1435–1441 (2012).
36. Levens, D. Disentangling the MYC web. *Proc Natl Acad Sci USA* **99,** 5757–5759 (2002).
37. Pellanda, P. *et al.* Integrated requirement of non-specific and sequence-specific DNA binding in Myc-driven transcription. *EMBO J* **40,** e105464 (2021).
38. Zeller, K. I., Jegga, A. G., Aronow, B. J., O'Donnell, K. A. & Dang, C. V. An integrated database of genes responsive to the Myc oncogenic transcription factor: identification of direct genomic targets. *Genome Biol.* **4,** R69–10 (2003).
39. Tulpule, A. *et al.* Kinase-mediated RAS signaling via membraneless cytoplasmic protein granules. *Cell* **184,** 2649–2664.e18 (2021).
40. Cai, D., Liu, Z. & Lippincott-Schwartz, J. Biomolecular Condensates and Their Links to Cancer Progression. *Trends Biochem Sci* 1–15 (2021). doi:10.1016/j.tibs.2021.01.002

41. Boija, A. Biomolecular condensates and cancer. *Cancer Cell* 1–19 (2021). doi:10.1016/j.ccell.2020.12.003
42. Tsang, B., Pritišanac, I., Scherer, S. W., Moses, A. M. & Forman-Kay, J. D. Phase Separation as a Missing Mechanism for Interpretation of Disease Mutations. *Cell* **183,** 1742–1756 (2020).
43. Jiang, S., Fagman, J. B., Chen, C., Alberti, S. & Liu, B. Protein phase separation and its role in tumorigenesis. *eLife* **9,** 647–27 (2020).
44. Sabari, B. R. Biomolecular Condensates and Gene Activation in Development and Disease. *Dev Cell* **55,** 84–96 (2020).
45. Wang, W. *et al.* Protein phase separation: A novel therapy for cancer? *Br J Pharmacol* **177,** 5008–5030 (2020).
46. Zhu, G. *et al.* Phase Separation of Disease-Associated SHP2 Mutants Underlies MAPK Hyperactivation. *Cell* 1–32 (2020). doi:10.1016/j.cell.2020.09.002
47. Brangwynne, C. P. *et al.* Germline P granules are liquid droplets that localize by controlled dissolution/condensation. *Science* **324,** 1729–1732 (2009).
48. Raccaud, M. & Suter, D. M. Transcription factor retention on mitotic chromosomes: regulatory mechanisms and impact on cell fate decisions. *FEBS Lett* **592,** 878–887 (2017).
49. Spencer, C. A., Kruhlak, M. J., Jenkins, H. L., Sun, X. & Bazett-Jones, D. P. Mitotic Transcription Repression in Vivo in the Absence of Nucleosomal Chromatin Condensation. *J Cell Biol* **150,** 13–26 (2000).
50. Gottesfeld, J. M. & Forbes, D. J. Mitotic repression of the transcriptional machinery. *Trends Biochem Sci* **22,** 197–202 (1997).

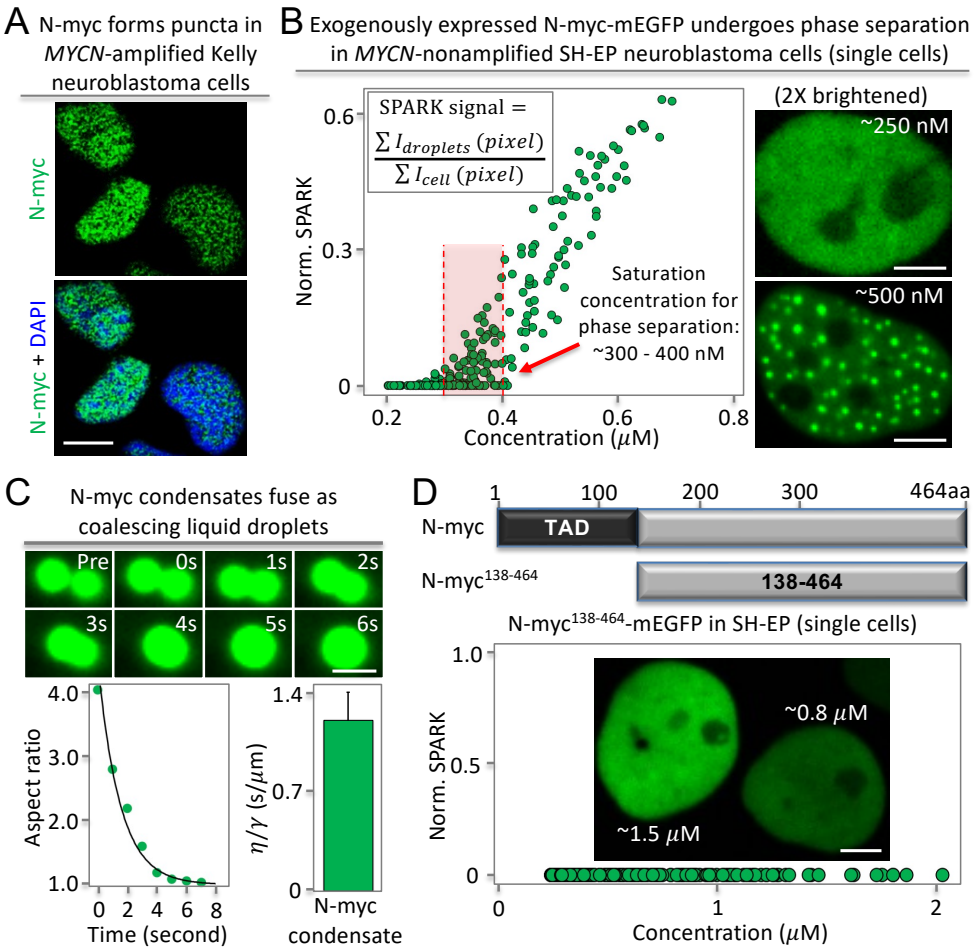

Fig. 1. N-myc undergoes liquid-liquid phase separation and requires the intrinsically disordered transactivation domain.
(A) Immunofluorescence images of N-myc in *MYCN*-amplified neuroblastoma Kelly cells. (B) Expression of mEGFP fused N-myc in the neuroblastoma SH-EP cells that have no or little endogenous N-myc protein expression. Left: quantitative analysis of N-myc puncta formation against its protein level in single cells. Each green circle corresponds to individual cells (~300 cells). The concentration of the fusion protein was estimated based on purified mEGFP (detailed in Methods). The red dashed line depicts saturation concentration for phase separation. Right: representative fluorescence images. (C) Fusion events between N-myc condensates. Top: fluorescence images. Bottom-left: quantitative analysis of the fusion events shown in the top. Bottom-right: inverse capillary velocity. Error bar represents standard deviation (n = 12). (D) Quantitative analysis of the truncated N-myc lacking N-terminal TAD that is an IDR. Each green circle corresponds to individual cells (~200 cells). Scale bars: 10 μm (A), 5 μm (B, D), 1 μm (C).

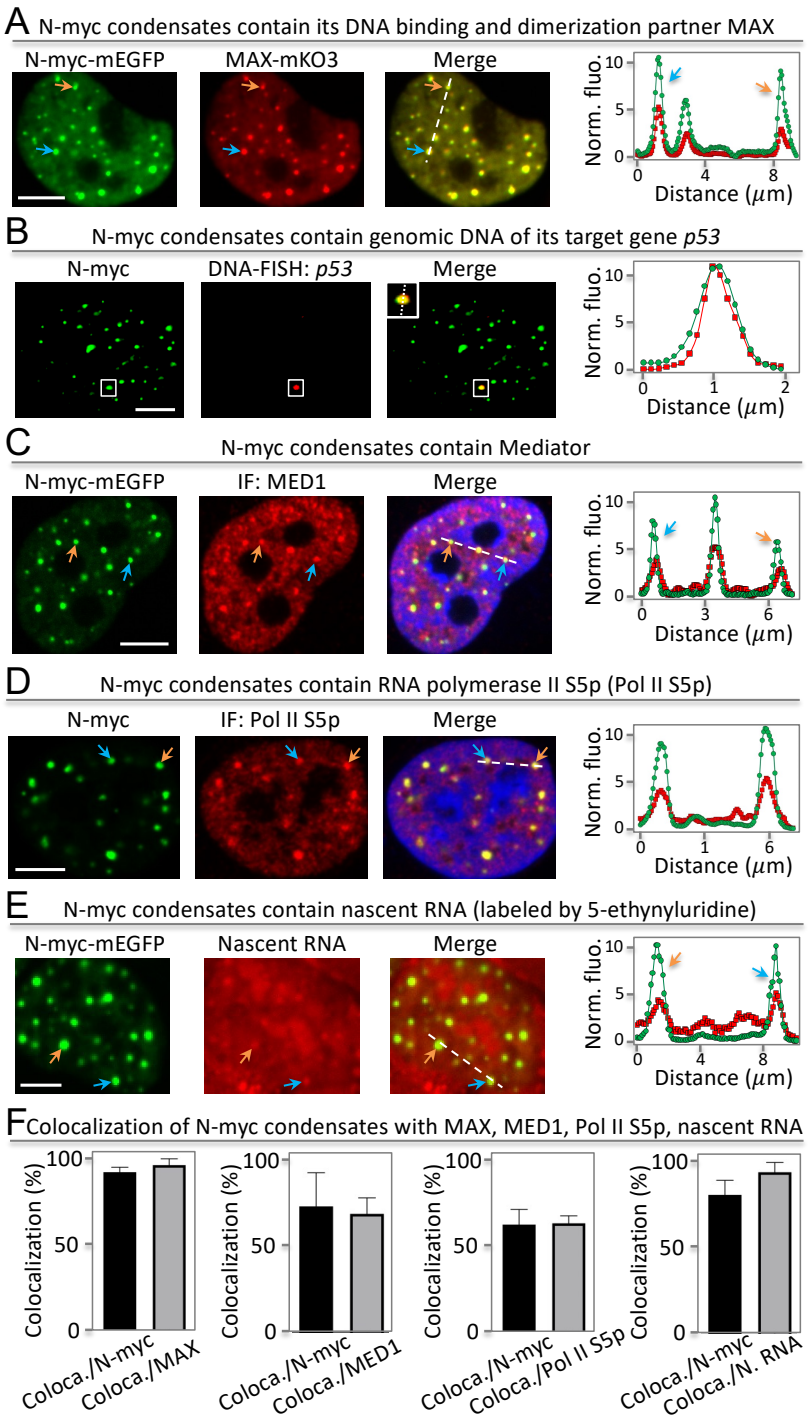

Fig. 2. N-myc condensates contain DNA-binding and dimerization partner, genomic DNA, transcriptional machinery and nascent RNA. (A) Fluorescent images of N-myc-mEGFP and MAX-mKO3 in SH-EP cells. The arrows point to representative condensates. The fluorescence intensity plot is shown on the right against position shown by the dashed line. (B) Fluorescence images of N-myc condensates with single molecule DNA FISH against *p53*. (C) Fluorescence images of N-myc condensates with immunofluorescence (IF)-imaged MED1. (D) Fluorescence images of N-myc condensates with immunofluorescence (IF)-imaged Pol II S5p. (E) Fluorescence images of N-myc condensates with nascent RNA labeled

Fig. 2. Legend (continued) by 5-ethynyluridine. (F) Percentage of N-myc condensates that colocalize with other condensates. The percentage is determined by the ratio of coloca./N-myc = number of colocalized condensates between N-myc and MAX divided by number of N-myc condensates. The same goes for other proteins. Data are mean ± SD (n = 13 cells). Scale bars, 5 μm (A – E).

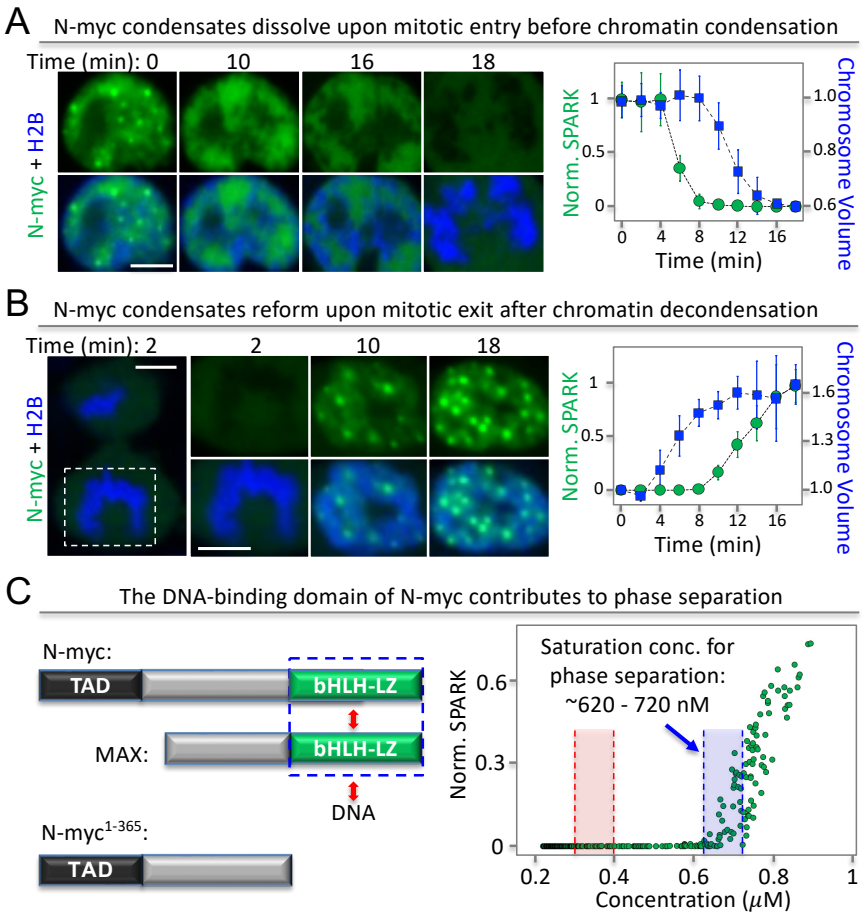

Fig. 3. Dynamic regulation of N-myc condensates during cell mitosis.
(A) Time-lapse images of SH-EP cells expressing N-myc-mEGFP upon mitotic entry. The cells co-expressed mIFP-tagged histone 2B (H2B, in blue). Chromosome volume was calculated based on mIFP-H2B fluorescence. Right panel: quantitative analysis of correlation between N-myc condensate dissolution and chromosome condensation. Error bar represents standard deviation (9 cells). (B) Time-lapse images of SH-EP cells expressing N-myc-mEGFP upon mitotic exit. Right panel: quantitative analysis of correlation between N-myc condensate reformation and chromosome de-condensation. Error bar represents standard deviation (7 cells). (C) Phase diagram of the truncated N-myc lacking the DNA-binding domain. The blue box depicts saturation concentration for N-myc$^{1\text{-}365}$ phase separation. The red box depicts saturation concentration for full length N-myc phase separation (see Fig. 1B).

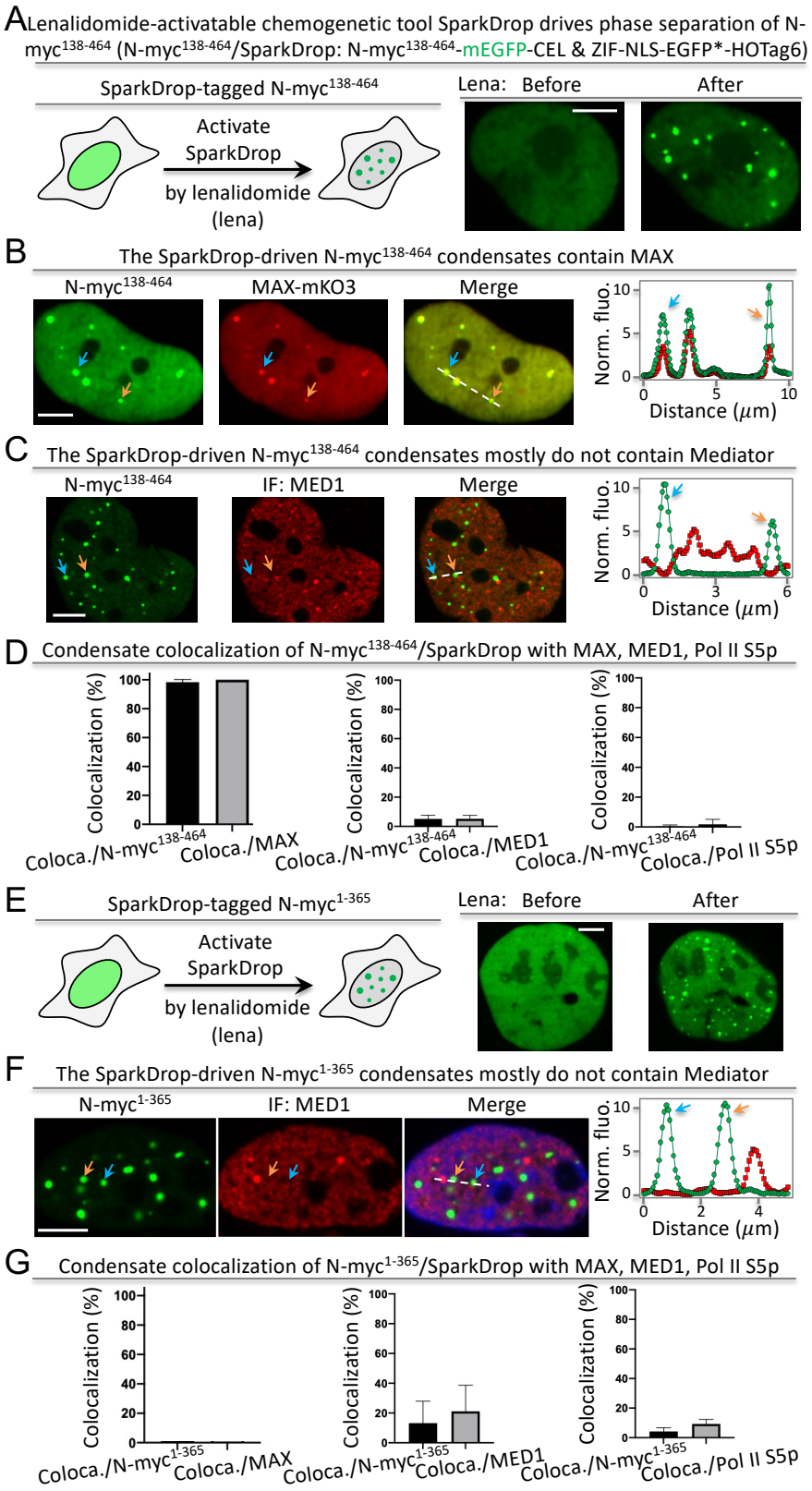

Fig. 4. Both TAD and DNA-binding domain are required for transcriptional activity of N-myc condensates. (A) Lenalidomide-activable SparkDrop drives phase separation of a

Fig. 4. Legend (continued) truncated N-myc lacking TAD. (B) Fluorescence images of N-myc$^{138-464}$/SparkDrop with MAX-mKO3. (C) Fluorescence images of SparkDrop-driven N-myc$^{138-464}$ condensates and MED1. (D) Percentage of N-myc$^{138-464}$/SparkDrop condensates that colocalize with other condensates. The percentage is determined by the ratio of coloca./N-myc$^{138-464}$ = number of colocalized condensates between N-myc$^{138-464}$/SparkDrop and MAX divided by number of N-myc$^{138-464}$/SparkDrop condensates. The same goes for other proteins. Data are mean ± SD (n = 15 cells). (E) Lenalidomide-activable SparkDrop drives phase separation of a truncated N-myc lacking DNA-binding domain. (F) Fluorescence images of SparkDrop-driven N-myc$^{1-365}$ condensates and MED1. (G) Percentage of N-myc$^{1-365}$/SparkDrop condensates that colocalize with other condensates. The percentage is determined by the ratio of coloca./N-myc$^{1-365}$ = number of colocalized condensates between N-myc$^{1-365}$/SparkDrop and MAX divided by number of N-myc$^{1-365}$/SparkDrop condensates. The same goes for other proteins. Data are mean ± SD (n = 15 cells). Scale bars: 5 μm (A – C, E, F).

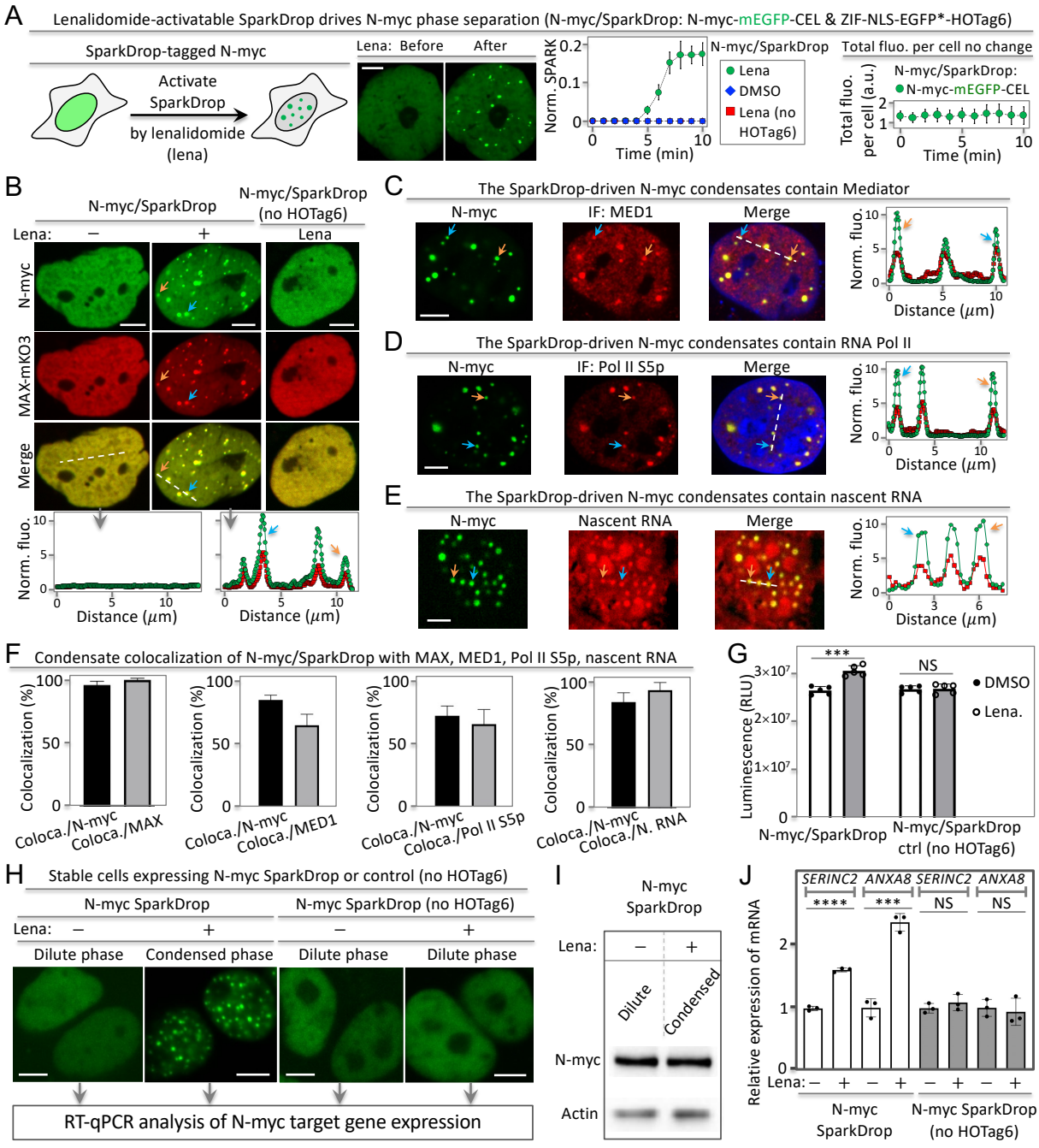

Fig. 5. The chemogenetic tool SparkDrop reveals role of phase separation of N-myc on transcription. (A) SparkDrop drives N-myc phase separation without change of protein level. (B) SparkDrop-driven N-myc condensates contain DNA-binding and dimerization partner MAX. (C – E) Fluorescence images showing SparkDrop-driven N-myc condensates contain transcriptional machinery including MED1 (C), RNA Pol II S5p (D), and nascent RNA (E). (F) Percentage of N-myc/SparkDrop condensates that colocalize with other condensates. The percentage is determined by the ratio of coloca./N-myc = number of colocalized condensates between N-myc/SparkDrop and MAX divided by number of N-myc/SparkDrop condensates. The same goes for other proteins including nascent RNA (N. RNA). Data are mean ± SD (n = 13 cells). (G) Quantitative analysis of SH-EP cell proliferation using CellTiter-Glo with N-myc

Fig. 5. Legend (continued) in dilute vs condensed phase. Luminescence was measured after the cells were treated with DMSO or lenalidomide (1μM) for 72 hrs. Data are mean ± SD (n = 5). *** P-value < 0.001. (H) Fluorescent images of stable cells expressing SparkDrop-tagged N-myc or the control. The cells were treated with lenalidomide or DMSO, followed by RT-qPCR analysis. (I) Western blot showing N-myc protein abundance level. (J) RT-qPCR analysis of two N-myc-regulated genes' expression level in the cells with condensed and dilute phase of N-myc. Data are mean ± SD (n = 3). ****P-value < 0.0001. *** P-value < 0.001. NS, not significant. Scale bars: 5 μm (A – E, H).

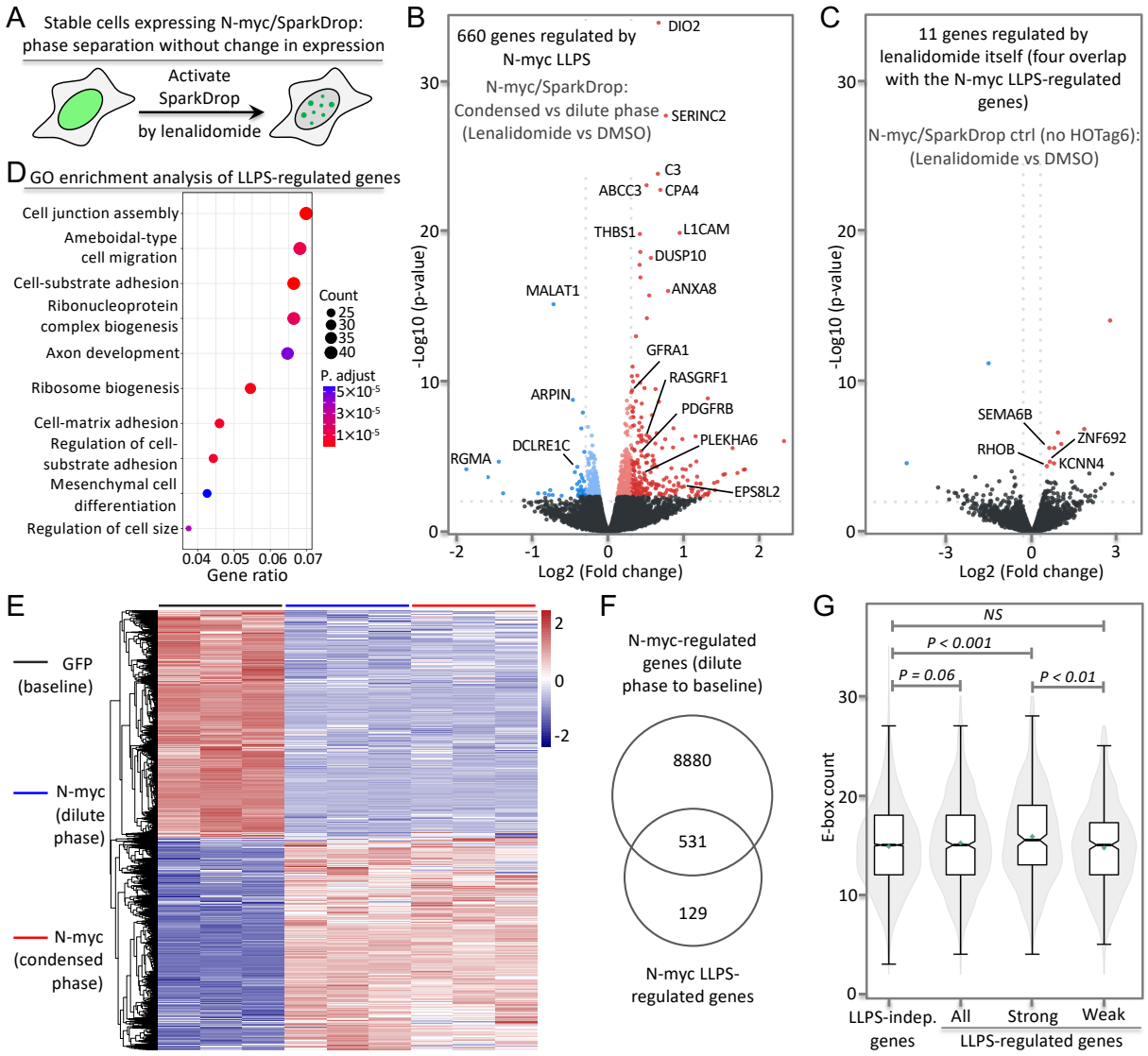

Fig. 6. Phase separation of N-myc differentially regulates transcriptome. (A) Schematic of SparkDrop-based N-myc phase separation without change of protein level. (B) Volcano plot showing fold change of mRNA levels (log2 fold change) for N-myc in the condensed to dilute phase (i.e. lenalidomide to DMSO) plotted against its p-value (−log10). mRNAs showing significant up- and down-regulation (p-value < 0.01, FDR < 0.1) are marked in red and blue, respectively. Black dots represent mRNAs with no significant changes. The DEGs with $|\log_2 FC| > 0.3$ or < 0.3 are categorized as strongly and weakly regulated groups, which are marked by solid and shaded colors, respectively. (C) Volcano plot showing fold change of mRNA levels for the N-myc SparkDrop control (no HOTag6) in lenalidomide to DMSO samples. mRNAs showing significant up- and down-regulation (p-value < 0.01, FDR < 0.1) are marked in red and blue, respectively. The four overlapped genes are labeled. See the full list in supporting excel file 4. (D) GO enrichment analysis of the N-myc LLPS-regulated genes. (E) Heat map showing mRNA levels of N-myc core genes that are significantly regulated. The number of the color key represents z-scores. (F) Venn diagram showing the overlap of N-myc-regulated genes (top, dilute phase) and the N-myc phase separation-regulated genes (bottom). (G) E-box enrichment analysis between the N-myc LLPS-

Fig. 6. Legend (continued) independent genes and the LLPS-regulated genes including strongly and weakly regulated groups. P values are indicated (Wilcoxon test). NS: not significant (p-value = 0.69).